

Atmospheric water transport connectivity within and between Ocean basins and land

Dipanjan Dey^{1,2,3}, Aitor Aldama Campino¹, and Kristofer Döös¹

¹Department of Meteorology, Stockholm University, 106 91 Stockholm, Sweden

²College of Engineering, Mathematics and Physical Sciences, University of Exeter, Exeter, UK

³School of Ocean and Earth Science, University of Southampton, Southampton, UK

Correspondence: Dipanjan Dey (dipanjanrocks01@gmail.com), Kristofer Döös (doos@misu.su.se)

Abstract. The global atmospheric water transport from the net evaporation to the net precipitation regions has been traced using Lagrangian trajectories. A matrix has been constructed by selecting various group of trajectories based on their surface starting (net evaporation) and ending (net precipitation) positions to show the connectivity of the 3-D atmospheric water transport within and between the three major ocean basins and the global landmass. The analysis reveals that a major portion of the net evaporated water precipitates back into the same region, namely 67% for the Indian, 64% for the Atlantic, 85% for the Pacific Ocean and 72% for the global landmass. It has also been calculated that 58% of the net terrestrial precipitation were sourced from the land evaporation. The net evaporation from the subtropical regions of the Indian, Atlantic and Pacific Oceans is found to be the primary source of atmospheric water for precipitation over the Intertropical Convergence Zone (ITCZ) in the corresponding basins. The net evaporated waters from the subtropical and western Indian Ocean were traced as the source for precipitation over the South Asian and Eastern African landmass, while Atlantic Ocean waters are responsible for rainfall over North Asia and Western Africa. Atlantic storm tracks were identified as the carrier of atmospheric water that precipitates over Europe, while the Pacific storm tracks were responsible for North American, eastern Asian and Australian precipitation. The bulk of South and Central American precipitation is found to have its source in the tropical Atlantic Ocean. The land-to-land atmospheric water transport is pronounced over the Amazon basin, western coast of South America, Congo basin, Northeastern Asia, Canada and Greenland. The ocean-to-land and land-to-ocean water transport through the atmosphere was computed to be $2 \times 10^9 \text{ kg s}^{-1}$ and $1 \times 10^9 \text{ kg s}^{-1}$, respectively. The difference between them (net ocean-to-land transport), i.e. $1 \times 10^9 \text{ kg s}^{-1}$, is transported to land. This net transport is approximately the same as found in previous estimates which were calculated from the global surface water budget.

1 Introduction

The hydrologic cycle traces the continuous movement of the water in the Earth system. The atmospheric hydrological cycle starts from the evaporation regions and ends in the precipitation regions. Generally evaporation tends to exceed precipitation over the ocean, while for land the opposite holds true. A consequence of this excess precipitation over land is that this surplus water eventually discharges into the ocean by the rivers, completing the atmospheric branch of the water cycle. The hydrological cycle is believed to strengthen in a future warmer climate. The Clausius-Clapeyron (CC) thermodynamic relation indicates that

25 for every 1°C temperature rise, the saturation vapour pressure will approximately increase by 7%. This implies that the vapour pressure, which is equivalent to the specific humidity or the amount of moisture in the atmosphere (Wallace and Hobbs, 2006), will also increase, as the tropospheric relative humidity is believed to remain the same in a warmer climate (Soden and Held, 2006). If the atmospheric circulation would remain unchanged, the water-vapour increase will solely act to intensify the moisture transport from the evaporation regions to the precipitation areas and help to magnify the strength of the existing global evaporation (E) - precipitation (P) patterns. This is the paradigm of “dry gets drier and wet gets wetter” or in other words “rich-get-richer mechanism” (Chou and Neelin, 2004). However, the increase of atmospheric moisture in a warmer climate does not necessarily imply that the global evaporation and precipitation will also increase by the same CC rate, as these are constrained by the surface energy budget (Held and Soden, 2006; Huntington, 2006). Analyses of future climate scenarios from Earth system models have revealed a 2-3% increase in global precipitation per 1°C temperature rise (Allan et al., 2014). 35 The imbalance between increasing rate of moisture and precipitation ensures that the precipitation intensity will increase in the future climate, while the frequency and duration are apt to decrease (Trenberth, 1999). In addition to this, the hydrologic cycle also plays a critical role in the global energy cycle through evaporative cooling of the Earth’s surface and latent heating of the atmosphere. The impact of the hydrologic cycle is not only important for the atmosphere but also for the ocean. The evaporation-dominated regions over the ocean generally leads to high salinity and the precipitation-dominated regions to low salinity. The Atlantic Ocean is e.g. a net freshwater flux surplus ($E - P > 0$) region in contrast to the Pacific Ocean, where the opposite holds true. This in turn gives rise to a salinity asymmetry, which can explain the generation of deep water in the North Atlantic but not in the North Pacific Ocean (Warren, 1983; Broecker et al., 1985; Emile-Geay et al., 2003). The North Atlantic Deep Water (NADW) is an integral part of the Atlantic Meridional Overturning Circulation (AMOC), which distributes heat within the climate system (Vellinga and Wood, 2008). It is projected by many climate models that the AMOC will weaken 40 during the 21st century, which could be linked to changes in the hydrologic cycle (Stocker et al., 2014).

Given these diverse roles of the hydrologic cycle within the Earth system, it is important to disentangle and understand its different parts. Previous studies were able to provide an estimate of the water storage in the reservoirs and also the net exchange of water between them using the surface water budgets (Chahine, 1992; Trenberth et al., 2007, 2011) (Chahine, 1992; Trenberth et al., 2007, 2011). The atmospheric water transport between the global ocean and land, the two dominating water reservoirs, are primarily obtained by integrating the net freshwater flux ($E - P$) over them. The integrated $E - P$ over the ocean is positive and calculated to be approximately 1 Sverdrups ($1 \text{ Sv} \equiv 10^9 \text{ kg s}^{-1} \equiv 0.031536 \equiv 31536 \text{ km}^3 \text{ year}^{-1}$, assuming water density is constant at 1000 kg m^{-3}), which is transported to land (Schmitt, 2008). Due to water-mass conservation this 1 Sv is equivalent to the negative $E - P$ integral over land (as $P > E$ over the land) and will return to the ocean through river discharges. The $E - P$ can either be directly obtained from the observationally based reanalysis data sets or derived from the moisture budget analysis (Trenberth et al., 2011). These kinds of studies suffer from the limitation that they can not provide information about the atmospheric water transport within and between different ocean basins and land. In addition, knowledge about how much of the ocean/land evaporated water precipitates over the ocean/land itself and is transported to the land/ocean is not achievable. However, these question will be possible to address using Eulerian/Lagrangian atmospheric water tracing schemes (Van der Ent et al., 2010; Tuinenburg et al., 2020; Stohl and James, 2004; Stein et al., 2015; Dey and Döös, 2020). A list of atmospheric 55

60 water tracing models and their advantages and disadvantages has been discussed briefly in Dominguez et al. (2020). The primary objective of the present study is to link 3-D atmospheric water transports within and between different ocean basins and land using Lagrangian trajectories, which makes it possible to trace water from the net evaporation at the surface to where it precipitates. This will facilitate the construction of an atmospheric freshwater connectivity matrix, which will provide both quantitative as well as qualitative descriptions of the 3-D atmospheric water exchange.

65 **2 Methods and data**

2.1 Lagrangian model for tracing water in the atmosphere

The mass conserving Lagrangian trajectory model TRACMASS v7.0 (Aldama-Campino et al., 2020; Döös, 1995) was used in the present study to obtain a detailed understanding of the global hydrologic cycle. One of the unique characteristics of TRACMASS is that it uses mass transports through the model grid box faces instead of velocity fields (Vries and Döös, 70 2001). TRACMASS was employed frequently to track the oceanic water-transport pathways (Berglund et al., 2017, 2021; Döös et al., 2008) and atmospheric air-mass routes (Kjellsson and Döös, 2012). In Dey and Döös (2020) TRACMASS was updated in order to trace water instead of air in the atmosphere. The atmospheric water tracing version of TRACMASS was also implemented recently to study the seasonal and inter-annual characteristics of the South Asian summer monsoon precipitation (Dey and Döös, 2021). Note here that these trajectory calculations are based on atmospheric water-mass transport in kg s^{-1} 75 and not transports of humid air. We are hence tracing the actual atmospheric water and not the moisture change along air-parcel trajectories. An elaborate evaluation of the atmospheric and oceanic trajectory schemes that are used in TRACMASS can be found in Döös et al. (2017).

The horizontal water transports through the model grid box faces are obtained by multiplying the air transports with its water content. The vertical water transport field is then obtained from an atmospheric water-mass conservation equation (Dey and 80 Döös, 2019), which is zero at the top of the atmosphere and equal to $E - P$ at each model level. The calculation of the vertical water transport from the conservation equation confirms that the evaporation, precipitation, condensation and advection of moisture by the winds are all summed up as the vertical water transport and cannot be separable. Note that the diffusive water transports, specific rain water and snow water content were omitted in Dey and Döös (2019, 2020), as well as in the present study due to its unavailability from the ERA-Interim but could be included in future studies. For a detailed mathematical 85 derivation of the atmospheric water transport see Dey and Döös (2019, 2020, 2021).

The mass conserving ability of TRACMASS (i.e. mass transport of a trajectory is conserved throughout its journey) has made it possible to compute Lagrangian stream functions from the simulated trajectories. The Lagrangian stream function is an useful tool to understand atmospheric and oceanic circulation pathways and has been used in previous studies extensively (Blanke et al., 1999; Berglund et al., 2017; Kjellsson and Döös, 2012; Döös et al., 2008). In the present study the Lagrangian 90 meridional and zonal overturning stream functions were computed to quantify atmospheric water-mass transport pathways in the meridional-vertical and zonal-vertical coordinate system respectively. The Lagrangian meridional overturning stream

function can be expressed as

$$\psi_{j,k} = \sum_{k'=k}^{kz} \sum_i \sum_m T_{i,j,k',m}^y, \quad (1)$$

here, i, j, k' are the zonal, meridional and vertical coordinates through which the trajectory indexed m passes. $T_{i,j,k',m}^y$ is the atmospheric water transport (kg s^{-1}) by the trajectory indexed m through the zonal-vertical grid box. The highest vertical level of the atmosphere is at 0.1 hPa and denoted as $k' = kz$. Note that the streamlines will be open and crossing the surface due to the sources (net evaporation) and sinks (net precipitation) of atmospheric water. Similarly, the Lagrangian zonal overturning stream function was computed as:

$$\psi_{i,k} = \sum_{k'=k}^{kz} \sum_j \sum_m T_{i,j,k',m}^x, \quad (2)$$

where $T_{i,j,k',m}^x$ is the Lagrangian water transport (kg s^{-1}) through the meridional-vertical grid-box face. The vertically integrated zonal ($F_{i,j}^x$) and meridional ($F_{i,j}^y$) water flux was computed from the 3-D simulated water trajectories to describe atmospheric water transport pathways in longitude-latitude framework:

$$F_{i,j}^x = \frac{\sum_{k'=0}^{kz} \sum_m T_{i,j,k',m}^x}{\Delta y_{i,j}}, \quad (3)$$

$$F_{i,j}^y = \frac{\sum_{k'=0}^{kz} \sum_m T_{i,j,k',m}^y}{\Delta x_{i,j}}. \quad (4)$$

The longitudinal and latitudinal grid spacing is denoted as Δx and Δy respectively. The resultant of the vertically integrated horizontal water flux is thus

$$F_{i,j} = \sqrt{(F_{i,j}^x)^2 + (F_{i,j}^y)^2}, \quad (5)$$

which has the unit Sv m^{-1} ($1 \text{ Sv} \equiv 10^9 \text{ kg s}^{-1}$). The calculated water trajectories were also used to compute atmospheric water residence time ($\tau_{i,j}$) following Dey and Döös (2020, 2021)

$$\tau_{i,j} = \frac{\sum_{m=1}^M \{(t_m^P - t_m^E) \cdot T_{i,j,m}^z\}}{\sum_{m=1}^M T_{i,j,m}^z}, \quad (6)$$

which is the lifetime of the atmospheric water between net evaporation and net precipitation. Here $T_{i,j,m}^z$ is the water transport of the trajectory indexed m through the surface. M is the total number of trajectories, t^P and t^E is the time when the atmospheric water trajectories precipitate and evaporate respectively.

2.2 Data source

The atmospheric water transports were computed using the surface pressure, specific humidity, specific cloud liquid and ice water content and horizontal wind velocities from the ERA-Interim reanalysis (Dee et al., 2011). The inclusion of the specific

cloud liquid and ice water content in the water transport calculation is an update as compared to the Dey and Döös (2020, 2021). The data sets were obtained for the years 2016 and 2017 with 0.75° spatial resolution, 6-hourly temporal resolution and 60 hybrid vertical model levels. It is noteworthy that to satisfy the mass conservation property of the Lagrangian model TRACMASS it requires data at model levels and not at interpolated pressure levels (Dey and Döös, 2021).

2.3 Lagrangian study configuration

To understand the 3-D global atmospheric water transport the Lagrangian trajectories were started over the entire surface of the globe when evaporation exceeded precipitation and followed until they reach back to the surface, which occurs when precipitation exceeded evaporation. These water trajectories were started at the surface every 6 hours during 2016 where $E > P$, then advected by the 3-D mass transport of water and followed until they reached back to the surface where $P > E$. In total more than 89 million water trajectories were started with more than 7 million trajectories each month. The position of a given atmospheric water trajectory within a grid box is solved analytically in space and with a stepwise-stationary scheme (Döös et al., 2017) in time. The trajectories were integrated in time with six intermediate time steps between each 6-hourly output data from the ERA-Interim. The trajectories were, however, followed for a maximum of one year. Only 0.4% remained in the atmosphere after one year and were subsequently discarded. The 3-D atmospheric water transport connection within and between different ocean basins and land, which can be regarded as an atmospheric water connectivity matrix, was estimated by sorting different classes of atmospheric trajectories based on their starting (net evaporation) and ending (net precipitation) positions. In the present study, the starting and ending points of the water trajectories were classified into the global landmass and the three major ocean basins as defined in Figure 1. The ocean basins are termed the Indian, Pacific, and the Atlantic Ocean (including the Arctic ocean).

3 Results

3.1 Atmospheric water connectivity

The atmospheric water is always on the move through space and in time within the climate system. In order to grasp the full characteristics of the atmospheric water circulation, it is thus necessary to reduce its dimensionality. The geographical connection of the atmospheric water transports within and between the ocean basins and the global landmass has been established by tracing the atmospheric water from the evaporation-dominated to the precipitation-dominated regions (Fig. 2), which are the starting and ending points of the trajectories. Additionally, a quantitative view of this geographical atmospheric water transport connection is presented in Table 1 by integrating the net evaporation/precipitation transport obtained from the sorted classes of trajectories. This integration of either net evaporation or precipitation will give the same result due to the mass-conserving property of the Lagrangian model TRACMASS. The atmospheric water movement in the horizontal-vertical plane is obtained by calculating the Lagrangian overturning water-mass stream functions using equation 1 and 2 and presented in latitude-pressure and longitude-pressure coordinate systems (Fig. 3 and Fig. 4 respectively). In addition, vertically integrated horizontal water

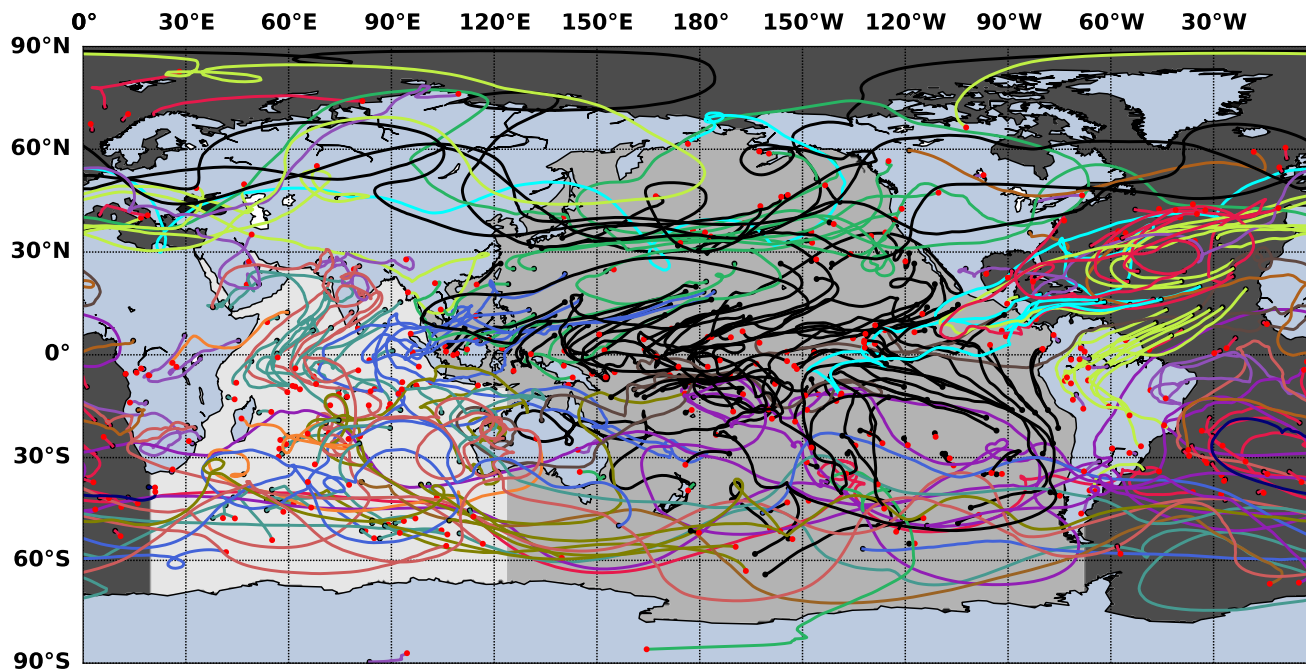


Figure 1. Spaghetti plot of few selected atmospheric water trajectories for the month of January 2016. The selected ocean basins are represented by different shadings of gray and defined as the Indian Ocean (IO), Pacific Ocean (PO) and Atlantic Ocean (AO). Note that, the Arctic Ocean is included in the Atlantic. The global landmass is taken as one single entity. The atmospheric water transport within and between the ocean basins and land has been calculated based on these defined sectors. The representative trajectories associated with these intra- and inter-basin water transport are labeled with different colors. The black dots are indicating the starting points and red points represent the ending points of the atmospheric water trajectories.

flux computation (using equation 5) is used to describe the water transport routes in longitude-latitude framework (Fig. 5). Note that the streamlines represent the integrated atmospheric water transport routes and is based on the sum of the Lagrangian trajectories, which should not be confused with the paths of the individual trajectories. Additionally, the streamlines start at the surface when $E > P$ and terminate where the opposite holds true. While interpreting the atmospheric water pathways from the meridional and zonal overturning stream functions, it should be remembered that these are zonally and meridionally integrated pathways respectively. For instance, the atmospheric water mass crossing a longitude can be transported zonally both by the tropical easterly trade winds and by the mid-latitude westerlies. If e.g. the westerlies transport more water than the easterlies at the same longitude then the meridionally integrated zonal overturning stream function will only show the dominant westerly signal. The residence time of the atmospheric water was mapped geographically at the net evaporation points using equation (6). This mapping was split up using the connectivity matrix so that the residence times indicate the inter- and intra-basin transport time scales (Fig. 6). This residence time was calculated at the points where net evaporation exceeds a monthly mean value of 0.2 mm day^{-1} in order to focus on the main source regions of the atmospheric water.

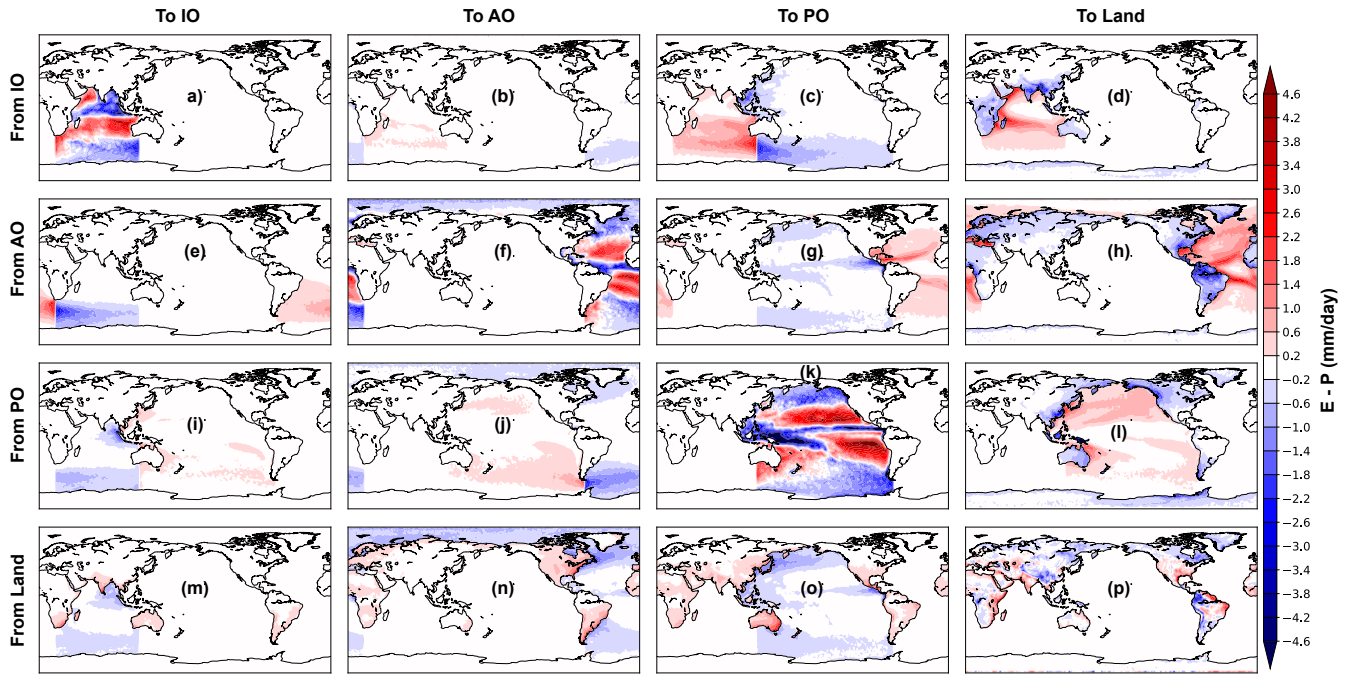


Figure 2. Annual mean $E - P$ (mm day^{-1}) inferred from the atmospheric waters travelling from the surface net evaporative regions (red contours) to the net precipitation areas (blue contours). The rows represent the net evaporative (starting points of the atmospheric water trajectories) sectors and the columns represent the net precipitation (ending points of the trajectories) regions.

Table 1. Atmospheric freshwater transport within and between the ocean basins and land. The rows represent net evaporative (atmospheric water source) sectors and the columns the net precipitation (atmospheric water sink) regions. Units are in Sv ($\equiv 10^9 \text{ kg s}^{-1}$). The percentages in the parentheses represent fractions of the net evaporation that are transported from the source region.

Regions	Indian Ocean	Atlantic Ocean	Pacific Ocean	Land
Indian Ocean	2.26 (67%)	0.10 (3%)	0.52 (15%)	0.52 (15%)
Atlantic Ocean	0.25 (5%)	3.07 (64%)	0.45 (9%)	1.07 (22%)
Pacific Ocean	0.23 (3%)	0.34 (4%)	7.52 (85%)	0.77 (8%)
Land	0.20 (5%)	0.48 (10%)	0.61 (13%)	3.30 (72%)

160 The results show that the net evaporation from the subtropical Atlantic, Pacific and Indian Ocean is the major source of water for net precipitation over the Intertropical Convergence Zone (ITCZ) in their respective basins (Fig. 2a, 2f and 2k). A major portion of the net evaporated water from the ocean basins was found to precipitate over their source sectors (Table 1). On an annual average, 67% (2.26 Sv), 64% (3.07 Sv) and 85% (7.52 Sv) of the net evaporation from the Indian, Atlantic and Pacific Ocean precipitates over the same oceanic basin (Table 1). The meridional overturning stream function and vertically

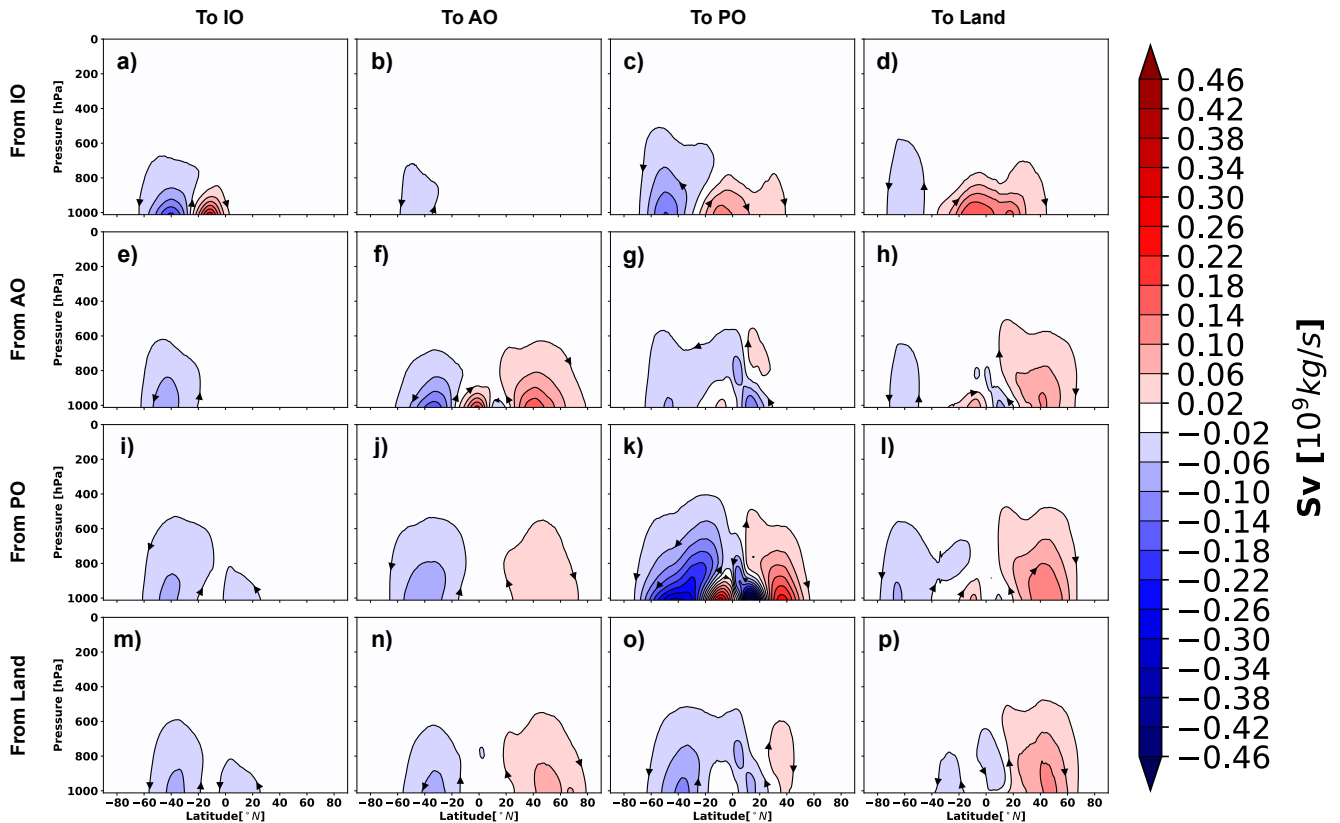


Figure 3. The Lagrangian meridional overturning stream function within and between the ocean basins and land. This has been undertaken by grouping the trajectories according to their starting and ending locations. The starting and ending points of the atmospheric trajectories are defined as per the sectors presented in Fig. 1. Note that the streamlines represent the integrated atmospheric water transport routes and is based on the sum of the Lagrangian trajectories, which should not be confused with the paths of the individual trajectories.

165 integrated horizontal water transport corresponding to these intra-basin atmospheric water transports (Fig. (3a; 5a), Fig. (3f; 5f) and Fig. (3k; 5k)) show that the Equatorward meridional transport in the Atlantic and the Pacific Oceans and northward transport in the Indian Ocean are dynamically responsible for most of the oceanic ITCZ rainfall. The easterly (east-to-west) water transport within the Pacific Ocean (blue cell in Fig. 4k and black lines in Fig. 5k) also plays a crucial role for the Pacific ITCZ precipitation and shows the atmospheric water movement within the Walker circulation. The evaporative waters from the Indian, Atlantic and Pacific Oceans stay on an average 4, 3 and 5 days, respectively, in the atmosphere before precipitating back into their basins of origin (Fig. 6a, 6f and 6k). Note that the residence-time map has a large spectrum of values and varies a lot within small distances in some of the defined regions, e.g. the evaporative water from the subtropical Pacific Ocean has residence time from 0 days to more than 24 days (Fig. 6k). The rainfall over the South Asian landmass and Eastern Africa is traced to originating and transporting mostly from the subtropical and Western Indian Ocean (Fig. 2d and Fig. 5d). Note that

170 this is an annual-mean figure and consists of precipitation signals from the entire year. The atmospheric water transport from

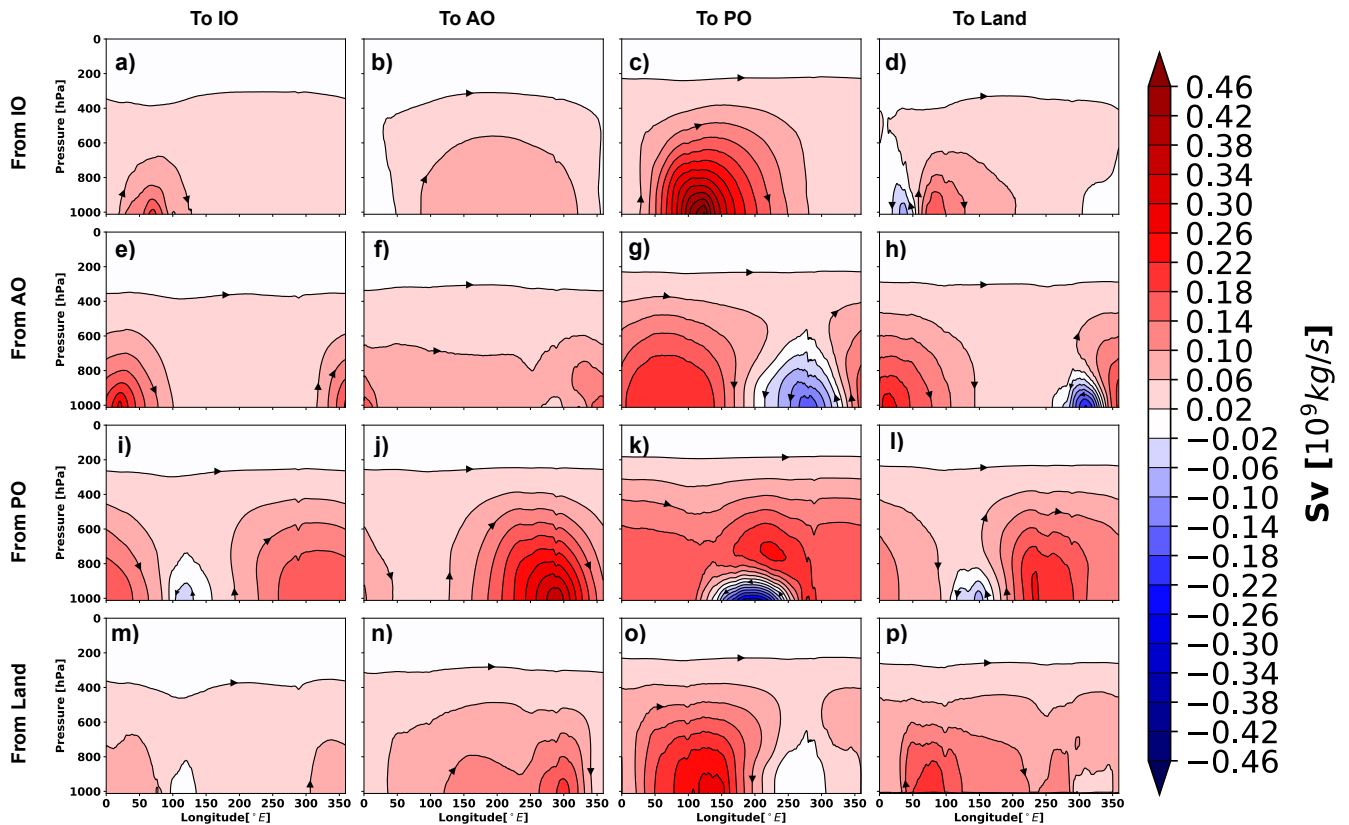


Figure 4. Same as Fig. 3 but for the zonal overturning stream function.

the Indian Ocean to the landmass is estimated to be around 0.52 Sv, which is 15% of the total Indian Ocean net evaporation (Table 1). The evaporated water from the Indian Ocean is primarily transported by the Somali low-level jet to the South Asian landmass. This low-level jet is a southwesterly flow which is active along the Somali coast during the summer monsoon months of June to September. The atmospheric water transport pathways associated with this jet is captured by the meridional and zonal overturning stream functions (Fig. 3d and Fig. 4d), in which the Northward (Fig. 3d) and Eastward (Fig. 4d) flow components carry atmospheric water to South Asia. Additionally, the horizontal water transport pathway from the Indian Ocean to the South Asian landmass by the Somali low-level jet is clearly noticeable in Fig. 5d.

The Easterly (Fig. 4d and Fig. 5d) component of the flow field transport water to Eastern Africa from the nearby Indian Ocean. The water that evaporated from the Indian Ocean and transported to land remains around 20 days in the atmosphere (Fig. 6d). The transport from the subtropical Atlantic Ocean to the tropical and mid-latitude Pacific Ocean (Fig. 2g) is found to be accomplished by the Easterly and Westerly winds, respectively, (Fig. 4g and Fig. 5g) and is calculated to be approximately 0.45 Sv (Table 1). The mean residence time of the evaporated waters from the Atlantic Ocean that are transported to the Pacific Ocean is 35 days (Fig. 6g). The majority of the South and Central American precipitation is found to be transported

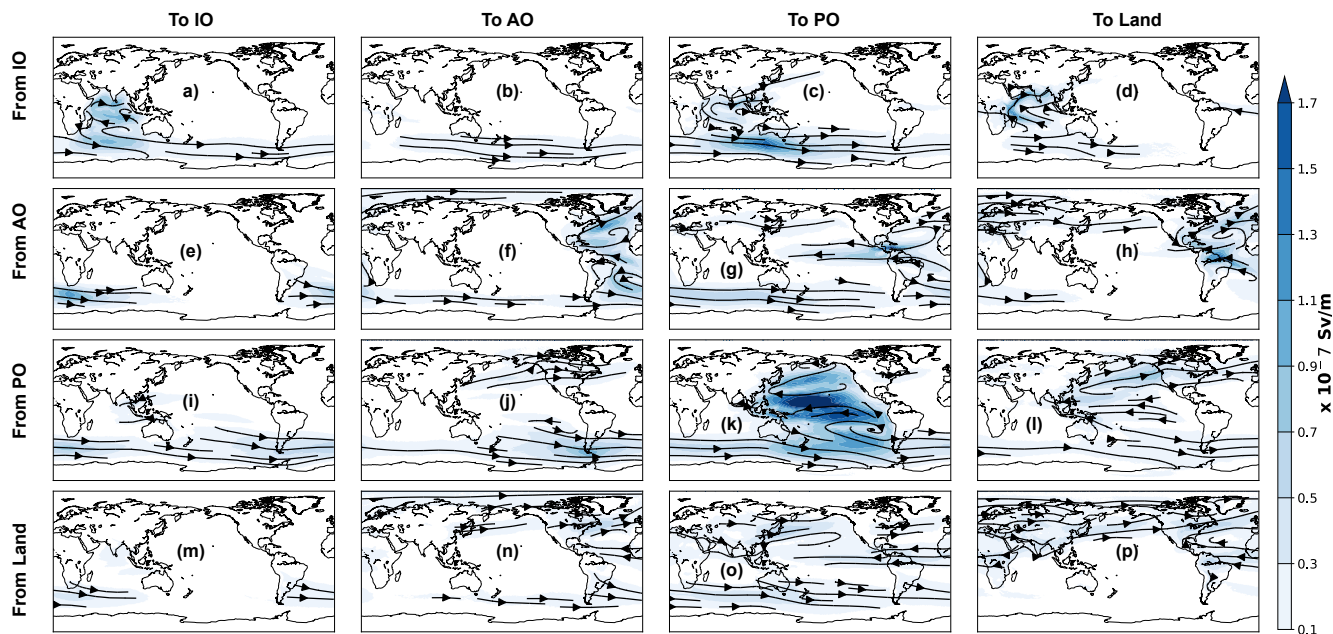


Figure 5. The vertically integrated horizontal water flux (shaded; Sv m^{-1}) within and between the ocean basins and land. This has been achieved by grouping the atmospheric water trajectories according to their starting and ending locations. The starting and ending points of the Lagrangian trajectories are defined as per the sectors presented in Fig. 1. The flux directions are given by the black lines.

from the tropical Atlantic (Fig. 2h) with the help of Easterly trade winds (blue cell in Fig. 4h and black lines in Fig. 5h). The Atlantic storm tracks, which orientated in an eastward direction, seemed to be responsible for the European and North Asian precipitation (Fig. 2h, 4h and 5h). The annual-mean Western African precipitation that is dominated by the Western African monsoon is traced to originating from the Atlantic Ocean and moves eastward (Fig. 2h and 4h). The winds over the Atlantic Ocean transport around 1.07 Sv atmospheric water to the land, which is 22% of its net evaporation (Table 1). The Atlantic Ocean evaporated waters stay in the atmosphere for 15 days before precipitating over Land (Fig. 6h). The rainfall over the west coast of North America, eastern coasts of Asia and Australia is primarily sourced from the Pacific Ocean (Fig. 2l) and its pattern closely resembles the pathways of the Pacific storm tracks. The total atmospheric water transport from the Pacific Ocean to the landmass is approximately 0.77 Sv (Table 1). The average residence time of the waters that are evaporated from the Pacific Ocean and precipitated over the landmass is found to be 21 days (Fig. 6l). The land to land atmospheric water transport is prominent over the Amazon basin, western coast of South America, Congo basin, the Northeastern sector of Asia, Canada and Greenland (Fig. 2p). The total amount of land-to-land atmospheric water transport is estimated to be around 3.30 Sv and is equal to 72% of its evapotranspiration, while 58% of the terrestrial precipitation were sourced from the land evaporation (Table 1). The evaporated water from land that falls back over the continents spends 6 days in the atmosphere (Fig. 6p). A spatial view of the global atmospheric water residence time (~~from both~~ mapped at the evaporation and precipitation perspective points) has been constructed from the Lagrangian water trajectories (Fig. S1) and discussed in the supplementary material (Text S1). The

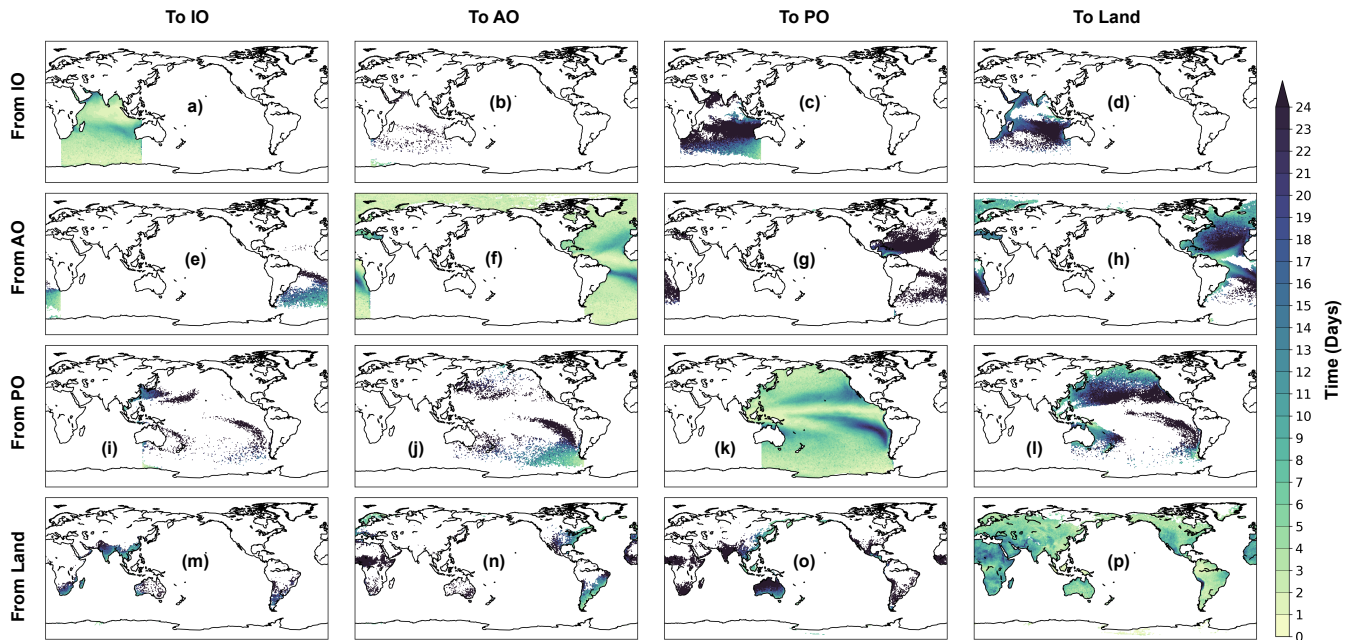


Figure 6. The average residence time (days) of the atmospheric waters mapped on their net evaporative points within and between the three ocean basins and land. Note that this has been mapped where the net evaporation exceeds a monthly mean value of 0.2 mm day^{-1} . The residence time has been calculated from the time the trajectories have spent in the atmosphere between their starting (net evaporation) and ending (net precipitation) points.

205 global average residence time of the atmospheric waters ~~from the evaporation and precipitation point of view is calculated to be around 7.5 days and 11 days respectively~~ is calculated (using equation 6) to be 9 days, which is similar to the estimate of 8 to 10 days by Van Der Ent and Tuinburg (2017) and the references therein.

3.2 A simplified quantitative view of the atmospheric water cycle

A simplified schematic of the annual mean global atmospheric water transports from both the surface water budget and La-
 210 grangian perspectives is presented in Fig. 7. It reflects the advantage of using a Lagrangian framework, from which ocean-to-ocean, ocean-to-land, land-to-land and land-to-ocean atmospheric water transport could be and was calculated (Fig. 7, bottom). The sketch was constructed by summing and rounding off the values of Table 1. For instance, net evaporation over the entire ocean was calculated by summing all the values of the atmospheric water transports from the defined ocean basins. The net evaporative transport from all the ocean basins is around 17 Sv, of which nearly 16 Sv precipitates over the ocean itself. The
 215 net ocean-to-land transport is thus 1 Sv, which returns to the ocean as runoff from land and equals the difference between the land net evaporation ($\approx 4.6 \text{ Sv}$) and land net precipitation ($\approx 5.6 \text{ Sv}$). It is found that 88% of the oceanic net evaporation (i.e. approximately 15 Sv) transported back to the ocean through precipitation. The ocean-to-land transport is computed to be

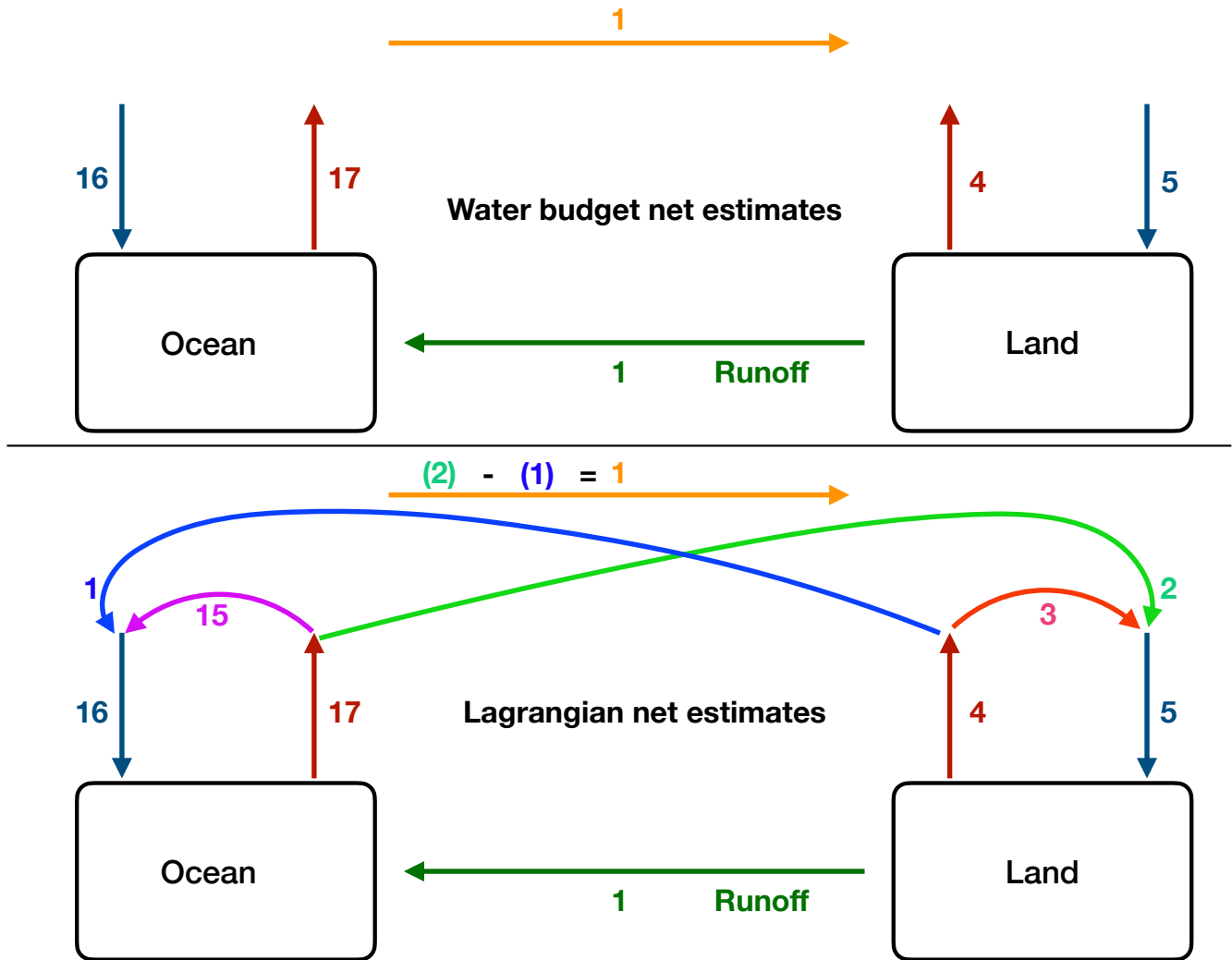


Figure 7. A sketch of the atmospheric water exchange between the Global Ocean and land. The top panel shows the surface water budget understanding of the hydrologic cycle, while the bottom panel elaborates the intricacies of the water movement that can be obtained using a Lagrangian framework. The upward and downward arrows represent net evaporation and net precipitation transport respectively. Note, the numbers presented here are the crudely estimated transports from Table 1 and have not been used for any quantification. Units are in Sverdrups ($1 \text{ Sv} \equiv 10^9 \text{ kg s}^{-1}$). It is important to mention that the net evaporation and net precipitation transports presented here are higher than the previous estimates such as Trenberth et al. (2007); Chahine (1992) and it might be due to the way $E - P$ has been computed in the present study which omits diffusive atmospheric water transport and time correlations.

around 2 Sv, while the land-to-ocean atmospheric water transport is approximately 1 Sv. The difference between them (i.e. 1 Sv) is the same as the net ocean-to-land water transport through the atmosphere one might obtain from an atmospheric surface

220 water budget point of view. The net land evapotranspiration is calculated to be around 4.6 Sv and 72% of this (i.e. around 3.3 Sv) goes into terrestrial precipitation. This estimate is similar to the estimate of 70% by Tuinenburg et al. (2020), which was based on the higher resolution ERA5 atmospheric reanalysis data during 2008 -2017 and a trajectory based moisture tracing model UTrack. However Link et al. (2020) and Van der Ent et al. (2010) reported a lower estimate of around 59% and 57% respectively while using the Eulerian numerical moisture tracking model Water Accounting Model (WAM), coarser
225 ERA-Interim data and different study period. The net land precipitation is estimated around 5.6 Sv and 58% of this (i.e. approximately 3.3 Sv) found to be originates from the land evaporation. This estimation is comparable with the Tuinenburg et al. (2020) study in which they noted that 51% of the global precipitation has evaporated from land. A study by Van der Ent et al. (2010) using WAM-1layer model [and ERA-Interim reanalysis product](#) reported that the continental precipitation recycling is 40%, an estimate lower than the present study. However using an updated moisture tracking model WAM-2layers [and land
230 evaporative fluxes from the Simple Terrestrial Evaporation to Atmosphere Model \(STEAM\)](#) Van der Ent et al. (2014) found that the continental precipitation recycling dropped to 36%.

The strength of the hydrological cycle in the present study is stronger than previous estimates such as [Chahine \(1992\); Trenberth et al. \(2007\)](#). ~~This despite~~ [Chahine \(1992\); Trenberth et al. \(2007\); Rodell et al. \(2015\) and others. For instance, the total global ocean evaporation was reported to be \$413 \times 10^3 \text{ km}^3 \text{ year}^{-1}\$ in Trenberth et al. \(2007\), \$434 \times 10^3 \text{ km}^3 \text{ year}^{-1}\$ in Chahine \(1992\), \$449.5 \pm 22.2\$
235 \$\times 10^3 \text{ km}^3 \text{ year}^{-1}\$ in Rodell et al. \(2015\), \$460 \times 10^3 \text{ km}^3 \text{ year}^{-1}\$ in Van Der Ent and Tuinenburg \(2017\) and in the current study the net evaporation has been computed to be around \$536 \times 10^3 \text{ km}^3 \text{ year}^{-1}\$ \(\$\approx 17 \text{ Sv}\$, calculated from Table 1\). The present study has calculated the net evaporation by taking only the points from the 6-hourly data where \$E - P > 0\$ and average over a year. Similarly the net precipitation in the present study has been estimated by considering only the points where \$E - P < 0\$. Thus one might expect ~~the opposite~~ \[a weaker hydrological cycle\]\(#\) since in the present study the atmospheric water is traced from
240 the net evaporation \(\$E - P > 0\$ \) to the net precipitation points \(\$E - P < 0\$ \) and not from the total evaporation \(\$E\$ \) to the total precipitation \(\$P\$ \). The reason for this could be explained by the way \$E - P\$ has been computed in the current study, which omits diffusive atmospheric water transports, specific rain and snow water content. Consider a hypothetical situation in which the vertical water transport computation without the diffusive water transport component leads to net precipitation and net evaporation regions adjacent to each other. Now, if we would include the diffusive water transport into the water-mass conservation
245 equation and for simplicity assume this addition would increase only the water transport through the connecting grid box face \(keeping all the other horizontal water transports constant as previous\) then the vertical water transport calculation would lead to a weaker net precipitation and net evaporation estimates. ~~Additional~~ \[An additional\]\(#\) reason might be related to the use of 6-hourly cumulative net freshwater transport in the present study, which prohibits the inclusion of processes occurring at ~~a
250 shorter timescale~~. \[shorter timescales, such as, time correlations between the wind speed and specific humidity. For an example, let us consider a grid box in which at time \\$t=0\\$ hrs the zonal wind is entering through its western wall with a velocity of \\$10 \text{ m s}^{-1}\\$ and specific humidity of \\$2 \text{ g kg}^{-1}\\$. The transport through all the other grid faces are assumed to be zero \\(for simplicity\\). This will lead to net precipitation transport of \\$20 \text{ m s}^{-1} \text{ g kg}^{-1}\\$ \\(to get a unit of \\$\text{kg s}^{-1}\\$ one has to multiply this quantity with \\$\Delta y \Delta z\\$ and water density\\). At time \\$t = 6\\$ hrs let's say the zonal wind strengthened to \\$20 \text{ m s}^{-1}\\$ but as wind increases the specific humidity decreases to \\$0.5 \text{ g kg}^{-1}\\$. This will lead to an net precipitation of \\$10 \text{ m s}^{-1} \text{ g kg}^{-1}\\$. Now if we average over these two\]\(#\)](#)

255 time steps we will get a net precipitation of $15 \text{ m s}^{-1} \text{ g kg}^{-1}$. However, averaging separately zonal wind and specific humidity will result in 15 m s^{-1} and 1.25 g kg^{-1} respectively and the net precipitation transport will thus be $\approx 19 \text{ m s}^{-1} \text{ g kg}^{-1}$. In the present study the 6-hourly average zonal wind and specific humidity was taken from the ERA-Interim separately (not the product of it) and thus the net evaporation and net precipitation amounts might be leading towards overestimation.

4 Conclusion and Discussion

260 One of the most striking and robust features of climate change is the acceleration of the atmospheric water cycle branch, which is associated with the temperature increase of the lower troposphere. In order to gain a detailed understanding of the future atmospheric water cycle and its importance, one should know the intricacies of the present-climate water cycle in the atmosphere. Although earlier studies were able to provide a quantification of the global atmospheric water cycle ~~but they missed a lot of~~ they missed detailed and important information which is essential to explain variations in continental water availability and near surface ocean salinity asymmetries. For instance, the global ocean-to-ocean, ~~total~~ ocean-to-land, ~~total~~ land-to-ocean and land-to-land water transport through the atmosphere were not extensively studied previously. Thus the global picture of the atmospheric water movement was incomplete. These shortcomings were overcome in the present study using a novel Lagrangian framework and presented a complete synthesised and quantitative view of the atmospheric water cycle. This Lagrangian methodology used in the present study made it possible to trace the atmospheric water transport from the net evaporation to the net precipitation regions within and between the different ocean basins and land. Earlier studies focused more on the regional or basin-scale surface water budget analysis (Alestalo, 1983; Yoon and Chen, 2005; Shi et al., 2014; Zheng et al., 2017; Liu et al., 2018) or continental water cycle (Van der Ent et al., 2010, 2014; Tuinenburg et al., 2020; Link et al., 2020), which could be viewed as a few pieces of a big puzzle. ~~Only a handful of studies were able to put forward a quantitative and synthesized view of the global atmospheric water cycle (Chahine, 1992; Browning and Gurney, 1999; Trenberth et al., 2007, 2011).~~ The atmospheric water transport quantification between two primary water reservoirs, e.g. ocean and land, is a straightforward issue to address. The residual between the integrated evaporation and precipitation over the ocean should be the net ocean-to-land transport and must be returned to the ocean as runoff. The water-mass conservation yields that this runoff should then be equal to the difference between the integrated evapotranspiration and precipitation over land. This concept has been elaborately demonstrated in Fig. 7 (top panel) and frequently been used previously in global quantification of the atmospheric water cycle (Chahine, 1992; Browning and Gurney, 1999; Trenberth et al., 2007, 2011; Rodell et al., 2015; Van Der Ent and Tuinenburg, 2017, & ref)

275 The surface water budget method suffers, however, from limitations as it can not provide any information about how much of the ocean/land evaporated water precipitates over the ocean/land itself and is transported to the land/ocean. However, these constraints were overcome in the present study by using Lagrangian water trajectories (Fig. 7, bottom panel). For example, in previous studies the net ocean-to-land water transport through the atmosphere was estimated to be around 1 Sv using the surface water budget method. This 1 Sv is practically the difference between the ocean-to-land ($\approx 2 \text{ Sv}$) and land-to-ocean ($\approx 1 \text{ Sv}$) transport, which is quantified in the present study.

285

The Eulerian/Lagrangian moisture tracking models that has been used in earlier studies were focused, in particular, on isolated aspects of the atmospheric hydrologic cycle, e.g. only ocean to river basin transport, land-to-land transport or some extreme precipitation events (Stohl and James, 2004, 2005; Stein et al., 2015; Van der Ent et al., 2010; Tuinenburg et al., 2020) (e.g., Stohl and
290 were also unable to provide the integrated water circulation pathways in the zonal-vertical or meridional-vertical framework. So, a complete 3-D picture of the atmospheric water transport connectivity within and between different ocean basins and land was missing. The sorting of the atmospheric water trajectories based on their starting and ending positions made it feasible to construct a map that shows the geographic connection of the atmospheric water transport from the net evaporative regions to the net precipitating areas (Fig. 2). It also reveals the integrated meridional, zonal and vertical transport pathways (Fig. 3, Fig.
295 4 and Fig. 5 respectively) of atmospheric water that travels within and between the defined ocean basins and the landmass. Further, an average atmospheric water residence time was presented (Fig. 6) which shows how long evaporated water from a particular location remains in the atmosphere before precipitating. The trajectory analysis indicates that 67% of the Indian Ocean net evaporation, 64% of the Atlantic Ocean net evaporation, 85% of the Pacific Ocean net evaporation and 72% of the land net evaporation precipitates back into the same region. The land-to-land atmospheric water transport is prominent over the
300 Amazon basin, western coast of South America, Congo basin, Northeastern Asia, Canada and Greenland. It has also been noted that 58% of the net terrestrial precipitation were sourced from the land evaporation. The net evaporation from the subtropical regions of the Indian, Atlantic and Pacific Oceans is found to be the major source of atmospheric water for ITCZ precipitation in the corresponding basins. The global average residence time of the atmospheric waters ~~from the evaporation and precipitation perspectives~~ was calculated to be ~~around 7.5 days and 11 days respectively.~~ 9 days. The strength of the atmospheric hydrologic
305 cycle in the present study is stronger than the earlier estimates and could be attributed to the omission of the diffusive water transports, specific rain and snow water content from the water-mass continuity equation and also to the processes occurring at time scale shorter than 6-hours. These limitations of the present method could be overcome by running the trajectory model on-line (i.e. calculating water trajectories simultaneously with the general circulation model run) with the inclusion of all the components of the water transport field. The present study has only used the advective fluxes of water but, if available, should
310 also include the diffusive fluxes of water, which could still be computed off-line.

In a warmer climate the atmospheric water transport is expected to be enhanced, which has far-reaching consequences. An extension of the present study could be to repeat a similar investigative strategy for future climate scenarios and identify how the atmospheric water transport within and between ocean basins and the landmass will change with respect to the present climate. The results could provide a detailed understanding of the future ocean salinity asymmetries as the ocean salinity is
315 closely tied to the surface evaporation and precipitation, which are the starting and ending points of the atmospheric water transport. Note that observational evidence of the oceanic salinity change already indirectly indicates a strengthening of the atmospheric branch of the water cycle (Durack and Wijffels, 2010). Additionally, future precipitation availability over the continents and the variability associated with it can also be mapped beforehand, and thus will be helpful for making strategies for the policymakers. The outcome of the present study is essential before pursuing any future climate studies regarding the
320 global atmospheric water cycle as it provides a complete global view of water transport through the atmosphere, which was missing earlier. The present study can be used as a springboard to launch and address future water-transport issues.

Code and data availability. The Lagrangian trajectory model TRACMASS v7.0 can be freely downloaded from <https://doi.org/10.5281/zenodo.4337926>. The ERA-Interim data at model levels are available from the ECMWF (<https://www.ecmwf.int/en/forecasts/datasets/archive-datasets/reanalysis-datasets/era-interim>) The trajectory model TRACMASS outputs that are used to plot the figures are freely accessible at <https://doi.org/10.5281/zenodo.5549573>. The analysis scripts are available on request from the corresponding author.

Author contributions. D. Dey and K. Döös conceptualized the study. D. Dey collected all the necessary data sets and employed the trajectory model TRACMASS. The outputs from the TRACMASS were analyzed by D. Dey with the programming help from A. Aldama Campino. The results were then discussed elaborately between all the authors. The manuscript is written by D. Dey with inputs from all the co-authors. A. Aldama Campino was responsible for the inclusion of the cloud liquid and ice water into the updated version of the TRACMASS.

330 *Competing interests.* No potential conflict of interest was reported by the authors.

Acknowledgements. The authors wish to acknowledge Peter Lundberg and Sara Berglund for their constructive comments. This work has been financially supported by the Swedish Research Council through grant agreement no. 2019-03574. The TRACMASS model integrations and the Lagrangian trajectory computations were performed on resources provided by the Swedish National Infrastructure for Computing (SNIC) at the National Supercomputer Centre (NSC) partially funded by the Swedish Research Council through grant agreement no. 2018-05973.

References

- Aldama-Campino, A., Döös, K., Kjellsson, J., and Jönsson, B.: TRACMASS: Formal release of version 7.0, <https://doi.org/10.5281/zenodo.4337926>, 2020.
- Alestalo, M.: The atmospheric water vapour budget over Europe, in: Variations in the global water budget, pp. 67–79, Springer, 1983.
- 340 Allan, R. P., Liu, C., Zahn, M., Lavers, D. A., Koukouvagias, E., and Bodas-Salcedo, A.: Physically consistent responses of the global atmospheric hydrological cycle in models and observations, *Surveys in Geophysics*, 35, 533–552, 2014.
- Berglund, S., Döös, K., and Nycander, J.: Lagrangian tracing of the water–mass transformations in the Atlantic Ocean, *Tellus A: Dynamic Meteorology and Oceanography*, 69, 1306–1311, 2017.
- Berglund, S., Döös, K., Campino, A. A., and Nycander, J.: The Water Mass Transformation in the Upper Limb of the Overturning Circulation
345 in the Southern Hemisphere, *Journal of Geophysical Research: Oceans*, 126, e2021JC017330, 2021.
- Blanke, B., Arhan, M., Madec, G., and Roche, S.: Warm water paths in the equatorial Atlantic as diagnosed with a general circulation model, *Journal of Physical Oceanography*, 29, 2753–2768, 1999.
- Broecker, W. S., Peteet, D. M., and Rind, D.: Does the ocean–atmosphere system have more than one stable mode of operation?, *Nature*, 315, 21–26, 1985.
- 350 Browning, K. A. and Gurney, R. J.: Global energy and water cycles, 1999.
- Chahine, M. T.: The hydrological cycle and its influence on climate, *Nature*, 359, 373–380, 1992.
- Chou, C. and Neelin, J. D.: Mechanisms of global warming impacts on regional tropical precipitation, *Journal of climate*, 17, 2688–2701, 2004.
- Dee, D. P., Uppala, S. M., Simmons, A., Berrisford, P., Poli, P., Kobayashi, S., Andrae, U., Balmaseda, M., Balsamo, G., Bauer, d. P., et al.:
355 The ERA-Interim reanalysis: Configuration and performance of the data assimilation system, *Quarterly Journal of the royal meteorological society*, 137, 553–597, 2011.
- Dey, D. and Döös, K.: The coupled ocean–atmosphere hydrologic cycle, *Tellus A: Dynamic Meteorology and Oceanography*, 71, 1650–1663, 2019.
- Dey, D. and Döös, K.: Atmospheric freshwater transport from the Atlantic to the Pacific Ocean: A Lagrangian analysis, *Geophysical Research
360 Letters*, 47, e2019GL086176, 2020.
- Dey, D. and Döös, K.: Tracing the origin of the South Asian summer monsoon precipitation and its variability using a novel Lagrangian framework, *Journal of Climate*, 34, 8655–8668, 2021.
- Dominguez, F., Hu, H., and Martinez, J.: Two-layer dynamic recycling model (2L-DRM): learning from moisture tracking models of different complexity, *Journal of Hydrometeorology*, 21, 3–16, 2020.
- 365 Döös, K.: Interocean exchange of water masses, *Journal of Geophysical Research: Oceans*, 100, 13499–13514, 1995.
- Döös, K., Nycander, J., and Coward, A. C.: Lagrangian decomposition of the Deacon Cell, *Journal of Geophysical Research: Oceans*, 113, 2008.
- Döös, K., Jönsson, B., and Kjellsson, J.: Evaluation of oceanic and atmospheric trajectory schemes in the TRACMASS trajectory model v6.0., *Geoscientific Model Development*, 10, 2017.
- 370 Durack, P. J. and Wijffels, S. E.: Fifty-year trends in global ocean salinities and their relationship to broad-scale warming, *Journal of Climate*, 23, 4342–4362, 2010.

- Emile-Geay, J., Cane, M. A., Naik, N., Seager, R., Clement, A. C., and van Geen, A.: Warren revisited: Atmospheric freshwater fluxes and “Why is no deep water formed in the North Pacific”, *Journal of Geophysical Research: Oceans*, 108, 2003.
- Held, I. M. and Soden, B. J.: Robust responses of the hydrological cycle to global warming, *Journal of climate*, 19, 5686–5699, 2006.
- 375 Huntington, T. G.: Evidence for intensification of the global water cycle: Review and synthesis, *Journal of Hydrology*, 319, 83–95, 2006.
- Kjellsson, J. and Döös, K.: Lagrangian decomposition of the Hadley and Ferrel cells, *Geophysical research letters*, 39, 2012.
- Link, A., Van Der Ent, R., Berger, M., Eisner, S., and Finkbeiner, M.: The fate of land evaporation—a global dataset, *Earth System Science Data*, 12, 1897–1912, 2020.
- Liu, W., Sun, F., Li, Y., Zhang, G., Sang, Y.-F., Lim, W. H., Liu, J., Wang, H., and Bai, P.: Investigating water budget dynamics in 18 river
 380 basins across the Tibetan Plateau through multiple datasets, *Hydrology and Earth System Sciences*, 22, 351–371, 2018.
- Rodell, M., Beaudoin, H. K., L’ecuyer, T., Olson, W. S., Famiglietti, J. S., Houser, P. R., Adler, R., Bosilovich, M. G., Clayson, C. A., Chambers, D., et al.: The observed state of the water cycle in the early twenty-first century, *Journal of Climate*, 28, 8289–8318, 2015.
- Schmitt, R. W.: Salinity and the global water cycle, *Oceanography*, 21, 12–19, 2008.
- Shi, F., Hao, Z., and Shao, Q.: The analysis of water vapor budget and its future change in the Yellow-Huai-Hai region of China, *Journal of
 385 Geophysical Research: Atmospheres*, 119, 10–702, 2014.
- Soden, B. J. and Held, I. M.: An assessment of climate feedbacks in coupled ocean–atmosphere models, *Journal of climate*, 19, 3354–3360, 2006.
- Stein, A., Draxler, R. R., Rolph, G. D., Stunder, B. J., Cohen, M., and Ngan, F.: NOAA’s HYSPLIT atmospheric transport and dispersion modeling system, *Bulletin of the American Meteorological Society*, 96, 2059–2077, 2015.
- 390 Stocker, T. F., Qin, D., Plattner, G.-K., Tignor, M. M., Allen, S. K., Boschung, J., Nauels, A., Xia, Y., Bex, V., and Midgley, P. M.: *Climate Change 2013: The physical science basis. contribution of working group I to the fifth assessment report of IPCC the intergovernmental panel on climate change*, 2014.
- Stohl, A. and James, P.: A Lagrangian analysis of the atmospheric branch of the global water cycle. Part I: Method description, validation, and demonstration for the August 2002 flooding in central Europe, *Journal of Hydrometeorology*, 5, 656–678, 2004.
- 395 Stohl, A. and James, P.: A Lagrangian analysis of the atmospheric branch of the global water cycle. Part II: Moisture transports between Earth’s ocean basins and river catchments, *Journal of Hydrometeorology*, 6, 961–984, 2005.
- Trenberth, K. E.: Conceptual framework for changes of extremes of the hydrological cycle with climate change, in: *Weather and climate extremes*, pp. 327–339, Springer, 1999.
- Trenberth, K. E., Smith, L., Qian, T., Dai, A., and Fasullo, J.: Estimates of the global water budget and its annual cycle using observational
 400 and model data, *Journal of Hydrometeorology*, 8, 758–769, 2007.
- Trenberth, K. E., Fasullo, J. T., and Mackaro, J.: Atmospheric moisture transports from ocean to land and global energy flows in reanalyses, *Journal of climate*, 24, 4907–4924, 2011.
- Tuinenburg, O. A., Theeuwens, J. J., and Staal, A.: High-resolution global atmospheric moisture connections from evaporation to precipitation, *Earth System Science Data*, 12, 3177–3188, 2020.
- 405 Van der Ent, R., Wang-Erlandsson, L., Keys, P. W., and Savenije, H.: Contrasting roles of interception and transpiration in the hydrological cycle—Part 2: Moisture recycling, *Earth System Dynamics*, 5, 471–489, 2014.
- Van Der Ent, R. J. and Tuinenburg, O. A.: The residence time of water in the atmosphere revisited, *Hydrology and Earth System Sciences*, 21, 779–790, 2017.

- Van der Ent, R. J., Savenije, H. H., Schaeffli, B., and Steele-Dunne, S. C.: Origin and fate of atmospheric moisture over continents, *Water Resources Research*, 46, 2010.
- 410 Vellinga, M. and Wood, R. A.: Impacts of thermohaline circulation shutdown in the twenty-first century, *Climatic Change*, 91, 43–63, 2008.
- Vries, P. and Döös, K.: Calculating Lagrangian trajectories using time-dependent velocity fields, *Journal of Atmospheric and Oceanic Technology*, 18, 1092–1101, 2001.
- Wallace, J. M. and Hobbs, P. V.: *Atmospheric science: an introductory survey*, vol. 92, Elsevier, 2006.
- 415 Warren, B. A.: Why is no deep water formed in the North Pacific?, *Journal of Marine Research*, 41, 327–347, 1983.
- Yoon, J.-H. and Chen, T.-C.: Water vapor budget of the Indian monsoon depression, *Tellus A: Dynamic Meteorology and Oceanography*, 57, 770–782, 2005.
- Zheng, Z., Ma, Z., Li, M., and Xia, J.: Regional water budgets and hydroclimatic trend variations in Xinjiang from 1951 to 2000, *Climatic Change*, 144, 447–460, 2017.